

Dynamic nuclear polarization and nuclear magnetic resonance in InSb quantum Hall ferromagnets

(Summary: Dynamic nuclear polarization has been demonstrated in the simplest pseudospin quantum Hall ferromagnet in a single InSb quantum well. This will advance our understanding of fundamental domain physics and provide a new way to unveil unique spin phenomena in narrow-gap nano-scale and layered structures.)

H. W. Liu^{1,2*}, K. F. Yang¹, T. D. Mishima³, M. B. Santos³ and Y. Hirayama^{1,4*}

¹ERATO Nuclear Spin Electronics Project, Sendai, Miyagi 980-8578, Japan

²State Key Lab of Superhard Materials and Institute of Atomic and Molecular Physics, Jilin University, Changchun 130012, P. R. China

³Homer L. Dodge Department of Physics and Astronomy, University of Oklahoma, Norman, OK 73019-2061, USA

⁴Department of Physics, Tohoku University, Sendai, Miyagi 980-8578, Japan

*e-mail: liuhw@ncspin.jst.go.jp; hirayama@m.tains.tohoku.ac.jp.

Studies of magnetic properties in a two-dimensional electron gas provide a powerful way to explore itinerant electron ferromagnetism. Rich physics is expected in this method involving tunable pseudospin (orbit, subband, and layer index) degrees of freedom. Here we characterize the simplest pseudospin quantum Hall ferromagnet with domain structures in single InSb quantum wells using resistively detected nuclear magnetic resonance. Dynamic nuclear polarization via the hyperfine interaction occurs when the domains with different pseudospin polarizations are energetically degenerate. Nuclear magnetic resonance signals of ¹¹⁵In (nuclear spin $I = 9/2$) are prominent, along with nine quadrupole splittings. The nuclear spin relaxation time T_1 is about 120 s, two orders of magnitude shorter than that of the bulk InSb,

suggesting that collective spin excitations may reside in the domain wall. These findings will advance our fundamental understanding of domain formation and unveil unique spin phenomena in narrow-gap quantum structures. The quadrupole-split spectra of ^{115}In provide the basis for coherent control of the ten nuclear-spin quantum levels and physical implementation of multiple quantum bits.

New and interesting subtleties in the integer quantum Hall effect (IQHE)¹ continue to emerge in the new century, with the discovery of quantum Hall ferromagnets (QHF) as a spectacular example^{2,3}. The study of magnetic properties in a two-dimensional electron gas (2DEG) is a powerful means to investigate the itinerant electron ferromagnetism (IEF) that is still a mystery in metallic systems⁴. In this method, interactions with the host material mostly occur with the effective mass (m^*) and effective Lande g factor (g^*) of electrons. In 2-D ferromagnets, the quantized single-particle states with macroscopically degenerate Landau levels (LLs) lead to intriguing prospects for the study of the IEF in combination with tunable pseudospin degrees of freedom involving the cyclotron orbital, quantum well (QW) subband, and layer indices. In a monolayer 2DEG, both ground (isotropic Heisenberg ferromagnet) and excited (topological charge, or ‘skyrmions’) spin states of the lowest LL at the filling factor (the number of occupied LLs) of $\nu = 1$ with real spins are described exactly by the Hartree-Fock (HF) theory, the $\nu = 1$ QHF is thus referred to as ‘the world’s best understood ferromagnet’².

Richer physics is expected in the field of 2-D ferromagnets when pseudospin degrees of freedom are taken into account^{5,6}. The simplest pseudospin QHF occurs at $\nu = 2$ in a monolayer 2DEG when the lowest two LLs with only orbital quantum numbers ($n = 0,1$) and spin indices ($\sigma = \uparrow, \downarrow$) intersect using tilted magnetic fields⁷. The $\nu = 2$ QHF is a simple ideal system for understanding the domain formation, which is crucial for studying the IEF. Magnetotransport measurements in various 2DEGs have hitherto demonstrated either hysteretic or non-hysteretic longitudinal resistance spikes (or peaks) in the $\nu = 2$ QHF, presumably arising from the interplay between disorder and domain morphology analogous to that in conventional magnets⁸⁻¹¹. However, traditional transport or optical measurements are not capable of addressing the nature of domain structures. More recently, the resistively detected nuclear magnetic resonance (RDNMR) technique, a local probe at the sites of nuclei, was shown to be an inherently sensitive way to study domains in a more complex QHF at fractional ν^{12} , where the LLs of strongly correlated electrons are described in the language of the IQHE with weakly interacting composite Fermions (CFs)¹³. The RDNMR measurement takes advantage of the hyperfine interaction which

supports electron-nuclear flip-flop, provided that energy is conserved. This emerging RDNMR technique has been also applied to probe exotic spin phenomena in nano-scale and layered structures¹⁴⁻²², which cannot be accomplished by other approaches. All RDNMR experiments have so far employed 2DEGs in GaAs, a host material in which electrons have a high electron mobility at low temperature and a small g^* (~ -0.44). However, the small g^* makes it difficult to form the simplest pseudospin QHF at $\nu = 2$ using easily achievable fields. Therefore, RDNMR measurements have not yet been performed in the $\nu = 2$ QHF.

Here we probe and characterize the simplest pseudospin QHF using the highly-sensitive RDNMR technique. The 2DEG sample in this work is a 30 nm wide InSb QW with symmetrically delta-doped $\text{Al}_{0.09}\text{In}_{0.91}\text{Sb}$ barriers grown by molecular beam epitaxy on a semi-insulating GaAs (001) substrate¹⁰. A Hall bar 170 μm in length and 40 μm in width is fabricated by conventional photolithography. Because the cyclotron energy $\hbar\omega_c = \hbar e B_{\perp} / m^*$ (\hbar is the reduced Planck's constant) between neighboring LLs depends on the component B_{\perp} of the total magnetic field (B_{tot}) normal to the plane of the 2DEG (Fig. 1a, θ is the tilt angle), while the spin (Zeeman) energy $\hbar\omega_s = g^* \mu_B B_{\text{tot}}$ (μ_B is the Bohr magneton and g^* is typically negative) depends on B_{tot} , the pseudospin-down $[(n, \sigma) = (0, \downarrow)]$ and pseudospin-up $[(n, \sigma) = (1, \uparrow)]$ sublevels will be brought close to degeneracy by tilting the 2DEG (called 'coincidence method'⁷, Fig. 1b). In this case, first-order phase transitions could occur from an unpolarized state $|(0, \uparrow), (0, \downarrow)\rangle$ to a fully polarized (ferromagnetic) state $|(0, \uparrow), (1, \uparrow)\rangle$, showing easy-axis (Ising) pseudospin anisotropy⁵. Disorder or finite temperature can produce a domain wall separating domains with different spin polarizations²³. As a typical narrow-gap semiconductor, the InSb-based 2DEG has extremely large g^* with a magnitude of up to 70²⁴. Therefore, the ratio $r = \hbar\omega_s / \hbar\omega_c = m^* g^* \mu_B / \hbar e \cos\theta$ is large, placing the LL degeneracy at experimentally accessible fields. This feature motivates the studies reported here on the InSb 2DEG sample. Our sample has a low-temperature electron mobility of $\mu = 14.3 \text{ m}^2/\text{Vs}$ and an electron density of $n_s = 1.83 \times 10^{15} \text{ m}^{-2}$.

RDNMR and tilted-magnetic-field measurements were performed using a dilution refrigerator with an

in-situ rotator. A low-frequency AC lock-in technique at 13.3 Hz was used to measure longitudinal resistances R_{xx} unless stated otherwise. A small radio-frequency (RF) field $\sim \mu\text{T}$ (continuous wave mode) matching the NMR frequency of individual isotopes was generated by a single turn coil wound around the Hall bar (Fig. 1a). To minimize heating effects, the sample was irradiated with a small RF power of -10 dbm.

A schematic diagram of the coincidence method is plotted in Fig. 1b, where B_{\perp} (or $\hbar\omega_c$) is kept constant for simplicity. As θ increases, B_{tot} (or $\hbar\omega_s$) increases and accordingly the LLs with different pseudospins (n, σ) intersect at integer ratios r . The intersections at a fixed r appear at the same angle when m^*g^* is constant. Such an LL evolution can be mapped by peak positions of R_{xx} measured at different θ . Figure 1c shows peak positions of R_{xx} vs. $1/\cos\theta$ and B_{\perp} (or ν) at a current of $I_{\text{sd}} = 3$ nA. The LLs are widely separated at high fields because $\hbar\omega_c$ increases with increasing B_{\perp} . The LL intersections (circle) with small spin polarization $\xi = r/\nu$ are characterized by a coalescence of R_{xx} minima. However, the LL intersections with high ξ show resistance spikes within persistent resistance minima (green line). The resistance spike is suggestive of a domain formation requiring a large exchange interaction⁶, consistent with the finding that the exchange energy E_{ex} is large at high ξ ²⁴. In addition, g^* is found to be enhanced by E_{ex} , reaching over 50 at these resistance spikes²⁴. The enhanced g^* indicates that the LL intersections move to smaller θ with decreasing ν at a fixed r (dashed line).

We first concentrate on the resistance spikes around $\nu = 2$. The dependence of R_{xx} on B_{\perp} at several angles is shown in Fig. 2a. The resistance spike between two LL peaks seems to lie between $\theta = 57.4^\circ$ and $\theta = 62.2^\circ$. However, this range of angles could be further extended by the RDNMR measurement. The resistance spike in the $\nu = 2$ QHF is non-hysteretic for different magnetic-field sweep directions, probably originating from domain stabilities⁹. Figure 2b shows R_{xx} vs B_{tot} over a range of I_{sd} . The peak R_{peak} of the resistance spike is found to increase with I_{sd} , which depends not only on electron transport across the QW (see below) but also on heating effects. Figure 2c shows R_{peak} at $B_{\text{tot}} = 7.5$ T vs temperature T and I_{sd} . Because T does not play a unique role in increasing R_{peak} , the T - R_{peak} data cannot be utilized to calibrate the effective temperature T_e induced by I_{sd} .

However, the T - R_{peak} curve can serve as an estimate of the upper limit of T_e . For instance, T_e should be less than 1.5 K for the typical current of $I_{\text{sd}} = 1.4 \mu\text{A}$ used in our RDNMR measurement.

We performed the RDNMR measurement on the resistance spikes in the $\nu = 2$ QHF. As a typical example, we chose the resistance spike at $\theta = 59.5^\circ$ (Fig. 2b). The measurement is initiated by sweeping B_{tot} to 7 T at $I_{\text{sd}} = 3 \text{ nA}$. Then, a large current of $1.4 \mu\text{A}$ is applied and time dependent R_{xx} is obtained (Fig. 3a). When R_{xx} becomes saturated, the RF field is set to irradiate the 2DEG while sweeping the frequency f through the Larmor resonance of individual nuclei. Figure 3b shows the R_{xx} vs. f for ^{115}In ($I = 9/2$) at an RF sweep rate of 20 kHz/min. A distinct dip characterized by a resistance change ΔR_{xx} appears at resonance frequency $f_{\text{NMR}} = 65.42 \text{ MHz}$, representing an RDNMR signal. Note that such an RDNMR signal can be detected even at 2 K using a helium-4 cryostat (data not shown). In a similar way, resonance signals of two nuclear isotopes of ^{121}Sb ($I = 5/2$) and ^{123}Sb ($I = 7/2$) are also obtained at $f_{\text{NMR}} = 71.38 \text{ MHz}$ and 38.64 MHz (Fig. 3c,d), respectively. The frequency f_{NMR} gives the gyromagnetic ratio $\gamma = 2\pi f_{\text{NMR}} / B_{\text{tot}}$ of the corresponding isotope: $\gamma_{^{115}\text{In}} = 58.7 \text{ MHz/T}$, $\gamma_{^{121}\text{Sb}} = 64 \text{ MHz/T}$ and $\gamma_{^{123}\text{Sb}} = 34.7 \text{ MHz/T}$ in accordance with those in the bulk InSb²⁵. The RDNMR signal of ^{113}In is not observed due to its low nuclear abundance (4.3%). As expected, no resonance is detected for ^{27}Al because the relevant nuclear spin polarization mainly occurs in the QW.

The RDNMR measurement relies on the hyperfine interaction. The contact hyperfine interaction $A\langle I_z \rangle S_z$ is dominant in InSb, where A is the hyperfine coupling constant, $\langle I_z \rangle$ is the nuclear spin polarization and S_z is the electron spin along the field direction²⁶. Because the energy cost for nuclear spin reversal is one-thousandth of that for electron spin reversal, the flip-flop requires a significant reduction in the energy change of the electron spin flip. At the intersection around $\nu = 2$, the domains with different pseudospin polarizations are energetically degenerate, thereby allowing for electron-nuclear spin reversal. When a relatively large current is applied, electrons move from one domain to the next and simultaneously polarize the relevant nuclei. Because the nuclear polarization only occurs at or near the domain walls with respect to the electron spin flip, the

distributions of the DNP sites are believed to be inhomogeneous. This DNP inhomogeneity induces additional domain disorder via the Overhauser shift¹², leading to extra dissipation between extended LL states and then increasing R_{xx} . By contrast, depolarization of nuclear spins at f_{NMR} reduces the domain disorder and hence results in a decrease of R_{xx} (Fig. 3b-d). Figure 3e shows the current dependent $\Delta R_{xx}/R_{xx}$ of ^{115}In , in which $\Delta R_{xx}/R_{xx}$ appears at $\sim 0.6 \mu\text{A}$ and increases with increasing I_{sd} but then decreases at higher I_{sd} . Because a large current could heat the sample, the decrease of $\Delta R_{xx}/R_{xx}$ at large I_{sd} should arise from heating effects. The data in Fig. 3e are indicative of a current-dependent DNP.

The regions with detectable RDNMR signals in the $\nu = 2$ QHF are mapped in Fig. 2a (filled circles and green traces). Apparently, the DNP only occurs around the resistance spikes. In particular, the highly-sensitive RDNMR approach allows us to probe the spikes hidden in the LL peaks and determine the real borders of the $\nu = 2$ QHF between $\theta = 53.2^\circ$ and $\theta = 64.3^\circ$. However, note that a hump rather than a dip is observed in the RDNMR signals of these two border spikes (Fig. 4b,d). In broad LL peaks, the polarized spike might shift relative to the unpolarized spike, with the result that the R_{xx} in one flank of the polarized spike is smaller than that of the unpolarized spike, probably accounting for the hump feature.

Further reducing the RF sweep rate (3 kHz/min) enables us to resolve the quadrupole splitting (Qs) of ^{115}In (Fig. 4a,b). The fit in Fig. 4b, as indicated by a red line composed of nine nearly equally spaced Gaussian curves, is in good agreement with the data. These nine curves are responsible for resonant transitions among ten quadrupole levels of ^{115}In ($I = 9/2$) with equal adjacent resonance intervals²⁷. In the simplest case of uniaxial strain along the growth direction, the splitting frequency of ~ 57 kHz (Fig. 4b) gives an estimate of deformation tensor element $e_{zz} \sim 0.2\%$, indicating less strain at relevant nuclear positions^{28,29}. This in principle coincides with our expectation that the lattice mismatch in the InSb QW is small ($\sim 0.7\%$). However, the strain analysis in the QHF becomes more complicated. In experiments, the Qs are found to decrease as the spike approaches $\nu = 2$ (~ 34 kHz, Fig. 4a) and become undistinguishable at $\nu = 1.48$ (Fig. 4d). More interestingly, the two sides of

the spike around $\nu = 2$ ($\theta = 59.5^\circ$, Fig. 2a) show different fine structures. Four resonance sublines can be resolved at $\nu = 2.12$ (Fig. 4a), but no notable sublines are observed at $\nu = 1.93$ (Fig. 4c). We suppose that such diverse properties of the Qs arise from the local strain at or near the domain walls where the DNP occurs, associated with their morphology, size, fluidity, and spatial distribution. Further theoretical and experimental studies of the strain in the QHF are expected to promote understanding of the domain formation. Note that this analysis does not take the influence of the Knight shift on the characteristics of the Qs²¹ into account because the Knight shift in InSb³⁰ is smaller than our measured Qs.

The T_1 measurement of ^{115}In is illustrated in the inset of Fig. 5a. When current-enhanced R_{xx} becomes saturated (Fig. 3a), the RF frequency is tuned to $f_{\text{NMR}} = 65.3$ MHz (on resonance). As a result of nuclear spin depolarization, R_{xx} decreases and then reaches a steady state. After that, f moves away from f_{NMR} (off resonance) and R_{xx} decays to the original value. The time dependence of R_{xx} at off-resonance follows a single exponential $R_{xx} \propto e^{-t/T_1}$, from which T_1 is determined³¹. Fig. 5a shows that T_1 does not exhibit any notable current dependence. Because a large current could heat the sample, the data in Fig. 5a also suggest that T_1 is almost temperature-independent, consistent with the observations in the ferromagnetic states of bilayer 2DEGs¹⁸ and two-sub-band monolayer 2DEGs²⁰. The average T_1 of 120 s, about two orders of magnitude shorter than that in the bulk InSb^{26,32}, indicates that collective spin excitations (skyrmion-like) responsible for significantly enhanced nuclear spin relaxation^{33,34} may reside in the domain wall. It is also worth noting that the spin-orbit (SO) interaction played a role in T_1 ³⁵. Based on the selection rules, the spin mixing at $r = 1$ is dominated by the Rashba SO term and the linear Dresselhaus SO term^{36,37}. The Rashba term can be neglected in symmetrically doped InSb QW¹⁰. The Dresselhaus term, however, may contribute to the reduced T_1 to some extent because the nuclear spins are expected to be randomized by mixing different LLs with opposite spins³⁵. Further experiments are needed to investigate the effect of the Dresselhaus SO coupling on the nuclear relaxation process, which is usually large in narrow-gap semiconductors. In addition, Fig. 5b plots T_1 at all spikes around $\nu = 2$ as a function

of B_{\perp} , where T_1 shows minima near $\nu = 2$ ($B_{\perp} \sim 3.8$ T) but obviously increases at $B_{\perp} > 4.5$ T (based on data from the border spike at $\theta = 53.2^\circ$ in Fig. 2a). At this point, we do not yet know the mechanism.

We further probed the DNP at the resistance spikes around $\nu = 3$ and $\nu = 4$ (Fig. 1c), but no RDNMR signals were observed. This is different from the observations at fractional ν where the RDNMR signals have been detected in the QHFs around filling factors $\nu^* = 2, 3$ and 4 of the CFs¹². Note that the QHFs at fractional ν occur at high B_{\perp} for a large ν^* of the CFs, while those in the IQHE move to low B_{\perp} with increasing ν . At low B_{\perp} (corresponding to a large magnetic length $\ell_B \sim \sqrt{1/B_{\perp}}$), the domain or domain wall size is expected to be large, and accordingly, the number of domains or domain walls participating in the electron spin flip decrease, which may account for the disappearance of the RDNMR signals at the $\nu = 3$ and $\nu = 4$ QHFs in the IQHE.

In addition, no RDNMR signals are observed at the other LL intersections marked with circles in Fig. 1c. Measurements of g^* in InSb QWs²⁴ suggest that the exchange interaction is responsible for the large gap at these intersections. However, the exchange coupling is not strong enough to support domain formation. Furthermore, we have proven that the thermal- or breakdown-induced nuclear polarization accessible in the GaAs QWs^{33,38} cannot be implemented at or near these intersections due to the large energy gap. Consequently, our experiments strongly suggest that the domain structures are required for electron-nuclear flip-flop at the LL intersection.

We have demonstrated the DNP in the simplest pseudospin QHF, which enables fundamental studies towards a physical understanding of the domain formation associated with the hyperfine coupling, exchange interaction, SO coupling, and local strain. The highly sensitive RDNMR and T_1 measurements developed in InSb QWs offer unique opportunities to investigate spin-related phenomena in quantum structures made of narrow-gap semiconductors characterized by a small effective mass, a strong SO interaction, large g factors, and band non-parabolicity, which play crucial roles in the emerging field of spintronics. Clear observations on the quadrupole splittings of ^{115}In support the possibility to coherently control the ten nuclear-spin quantum levels

and build multiple NMR-based quantum bits (≥ 2). The developed quadrupole split spectra are expected to probe local strains in In-based heterostructures and nanostructures as alternative device technologies beyond Si complementary metal–oxide–semiconductor (CMOS).

References

1. Klitzing, K. v., Dorda, G. & Pepper, M. New method for high-accuracy determination of the fine-structure constant based on quantized hall resistance. *Phys. Rev. Lett.* **45**, 494 (1980).
2. Girvin, S. M. Spin and isospin: Exotic order in quantum Hall ferromagnets. *Phys. Today* **53**, 39 (2000).
3. Ezawa, Z. F. & Tsitsishvili, G. Quantum Hall ferromagnets. *Rep. Prog. Phys.* **72**, 1 (2009).
4. De Poortere, E. P., Tutuc, E., Papadakis, S. J. & Shayegan, M. Resistance spikes at transitions between quantum Hall ferromagnets. *Science* **290**, 1546 (2000).
5. Jungwirth, T. & MacDonald, A. H. Pseudospin anisotropy classification of quantum Hall ferromagnets. *Phys. Rev. B* **63**, 035305 (2000).
6. Jungwirth, T. & MacDonald, A. H. Resistance spikes and domain wall loops in Ising quantum Hall ferromagnets. *Phys. Rev. Lett.* **87**, 216801 (2001).
7. Nicholas, R. J., Haug, R. J., Klitzing, K. v. & Weimann, G. Exchange enhancement of the spin splitting in a GaAs-Ga_xAl_{1-x}As heterojunction. *Phys. Rev. B* **37**, 1294 (1988).
8. Jaroszyński, J. *et al.* Ising quantum hall ferromagnet in magnetically doped quantum wells. *Phys. Rev. Lett.* **89**, 266802 (2002).
9. Gusev, G. M., Quivy, A. A., Lamas, T. E. & Leite, J. R. Quantum Hall ferromagnet in a parabolic well. *Phys. Rev. B* **67**, 155313 (2003).
10. Chokomakoua, J. C. *et al.* Ising quantum Hall ferromagnetism in InSb-based two-dimensional electronic systems. *Phys. Rev. B* **69**, 235315 (2004).
11. Vakili, K. *et al.* Spin-dependent resistivity at transitions between integer quantum Hall states. *Phys. Rev. Lett.* **94**, 176402 (2005).
12. Stern, O. *et al.* NMR study of the electron spin polarization in the fractional quantum Hall effect of a single quantum well: Spectroscopic evidence for domain formation. *Phys. Rev. B* **70**, 075318 (2004).

13. Jain, J. K. Composite-fermion approach for the fractional quantum Hall effect. *Phys. Rev. Lett.* **63**, 199 (1989).
14. Kronmüller, S. *et al.* New type of electron nuclear-spin interaction from resistively detected *Phys. Rev. Lett.* **82**, 4070 (1999).
15. Smet, J. H. *et al.* Gate-voltage control of spin interactions between electrons and nuclei in a semiconductor. *Nature* **415**, 281 (2002).
16. Hashimoto, K., Muraki, K., Saku, T. & Hirayama, Y. Electrically controlled nuclear spin polarization and relaxation by quantum-Hall states. *Phys. Rev. Lett.* **88**, 176601 (2002).
17. Yusa, G., Muraki, K., Takashina, K., Hashimoto, K. & Hirayama, Y. Controlled multiple quantum coherences of nuclear spins in a nanometer-scale device. *Nature* **434**, 1001 (2005).
18. Kumada, N., Muraki, K. & Hirayama, Y. Low-frequency spin dynamics in a canted antiferromagnet. *Science* **313**, 329 (2006).
19. Tracy, L. A., Eisenstein, J. P., Pfeiffer, L. N. & West, K. W. Spin transition in the half-filled Landau level. *Phys. Rev. Lett.* **98**, 086801 (2007).
20. Zhang, X. C., Scott, G. D. & Jiang, H. W. NMR probing of spin excitations in the ring structure of a two-subband system. *Phys. Rev. Lett.* **98**, 246802 (2007).
21. Kumada, N., Muraki, K. & Hirayama, Y. NMR evidence for spin canting in a bilayer $\nu = 2$ quantum Hall system. *Phys. Rev. Lett.* **99**, 076805 (2007).
22. Hirayama, Y., Yusa, G., Hashimoto, K., Kumada, N., Ota, T. & Muraki, K. Electron-spin/nuclear-spin interactions and NMR in semiconductors. *Semicon. Sci. Technol.* **24**, 023001(2009).
23. Brey, L. & Tejedor, C. Spins, charges, and currents at domain walls in a quantum Hall Ising ferromagnet. *Phys. Rev. B* **66**, 041308 (R) (2002).
24. Nedniyom, B. *et al.* Giant enhanced g -factors in an InSb two-dimensional gas. *Phys. Rev. B* **80**, 125328

(2009).

25. Clark, W. G. & Feher, G. Nuclear polarization in InSb by a dc current. *Phys. Rev. Lett.* **10**, 134 (1963).
26. Gueron, M. Density of conduction electrons at nuclei in indium antimonide. *Phys. Rev. A* **135**, A200 (1964).
27. Sundfors, R. K. Exchange and quadrupole broadening of nuclear acoustic resonance line shapes in the III-V semiconductors. *Phys. Rev.* **185**, 458 (1969).
28. Sundfors, R. K. Experimental gradient-elastic tensors and chemical bonding in III-V semiconductors. *Phys. Rev. B* **10**, 4244 (1974).
29. Dzhioev, R. I. & Korenev, V. L. Stabilization of the electron-nuclear spin orientation in quantum dots by the nuclear quadrupole interaction. *Phys. Rev. Lett.* **99**, 037401 (2007).
30. Tunstall, D. P. The knight-shift in doped indium arsenide and in doped indium-antimonide in the extreme quantum limit. *J. Phys. C* **21**, 2853 (1988).
31. Gervais, G. *et al.* Evidence of Skyrmion crystallization from NMR relaxation experiments. *Phys. Rev. Lett.* **94**, 196803 (2005).
32. Gauss, N., Jansen, A. G. M. & Wyder, P. Effect of nuclear field on magnetotransport quantum oscillations in InSb. *J. Supercond.* **17**, 653 (2004).
33. Desrat, W. *et al.* Resistively detected nuclear magnetic resonance in the quantum Hall regime: Possible evidence for a Skyrme crystal. *Phys. Rev. Lett.* **88**, 256807 (2002).
34. Côté, R. *et al.* Collective excitations, NMR, and Phase transitions in Skyrme crystals. *Phys. Rev. Lett.* **78**, 4825 (1997).
35. Hashimoto, K., Muraki, K., Kumada, N., Saku, T. & Hirayama, Y. Effects of inversion asymmetry on electron-nuclear spin coupling in semiconductor heterostructures: Possible role of spin-orbit interactions. *Phys. Rev. Lett.* **94**, 146601 (2005).
36. Das, B., Datta, S. & Reifengerger, R. Zero-field spin splitting in a two-dimensional electron gas. *Phys. Rev.*

B **41**, 8278 (1990).

37. Schliemann, J., Egues, J. C. & Loss, D. Variational study of the $\nu = 1$ quantum Hall ferromagnet in the presence of spin-orbit interaction. *Phys. Rev. B* **67**, 085302 (2003).

38. Kawamura, M. *et al.* Electrical polarization of nuclear spins in a breakdown regime of quantum Hall effect. *Appl. Phys. Lett.* **90**, 022102 (2007).

Acknowledgements

We acknowledge helpful discussions with K. Hashimoto, S. Watanabe, K. Muraki, and N. Shibata. H.W.L. thanks the Program for New Century Excellent Talents of University in China.

Author contributions

H.W.L. and Y.H. planned the experiment. K.F.Y. and H.W.L. carried out the measurements and analyzed the data. T.D.M. and M.B.S. fabricated the sample. H.W.L. prepared the manuscript.

Figure 1 | Tilted magnetic field experiments. **a**, Tilt angle θ between the total magnetic field B_{tot} and its component B_{\perp} normal to the 2DEG plane. A single turn coil generates RF fields. **b**, Schematic LL intersections at constant cyclotron energy of $\hbar\omega_c$. Indices (n, σ) label relevant pseudospin levels and integer numbers denote ν . The Zeeman energy $\hbar\omega_s$ increases with increasing θ , leading to the LL degeneracy at an integer ratio r . **c**, Peak positions of longitudinal resistance R_{xx} vs. B_{\perp} (or filling factor ν) and $1/\cos\theta$ at $I_{\text{sd}} = 3$ nA and $T = 200$ mK. One type of the LL intersection in the data is characterized by a merged R_{xx} peak and marked with a circle, while the other type is featured in a resistance spike and accentuated by a green line.

Figure 2 | Temperature and current dependence of longitudinal resistance R_{xx} and distributions of RDNMR signals in the $\nu = 2$ pseudospin QHF. **a**, R_{xx} as a function of B_{\perp} at several angles (data derived from Fig. 1). The curves are offset for clarity. Filled circles together with green traces around the resistance spikes map the RDNMR regions. The diameter of filled circles denotes the ratio between the DNP-induced resistance change ΔR_{xx} and R_{xx} of ^{115}In . **b**, R_{xx} at $\theta = 59.5^\circ$ as a function of B_{tot} at different I with constant intervals of 0.25 μA . **c**, Dependence of the spike peak R_{peak} on T and I_{sd} at $\theta = 59.5^\circ$ and $B_{\text{tot}} = 7.5$ T. The red line is a fit following $\exp(-\sqrt{T_0/T})$ behavior with $T_0 = 25.6$ K, suggestive of hopping transport.

Figure 3 | RDNMR signals of In and Sb nuclei. **a**, Time dependence of R_{xx} at $\theta = 59.5^\circ$, $B_{\text{tot}} = 7$ T, and $T = 100$ mK after I_{sd} changes from 3 nA to 1.4 μA . As R_{xx} becomes saturated, the RDNMR measurement sets in. **b**, RDNMR signal of ^{115}In measured at an RF sweep rate of 20 kHz/min. **c,d**, RDNMR signals of ^{121}Sb and ^{123}Sb obtained using an AC resistance bridge with an excitation current of 1 μA at 3 kHz/min. **e**, $\Delta R_{xx}/R_{xx}$ of ^{115}In as a function of I_{sd} .

Figure 4 | Quadrupole splittings of ^{115}In . **a-d**, RDNMR signals of ^{115}In at several positions in the $\nu = 2$ QHF with a slow RF sweep rate of 3 kHz/min, $I_{\text{sd}} = 1.4$ μA , and $T = 100$ mK. The red line in **b** is a fit with nine Gaussian curves (green color).

Figure 5 | Nuclear spin relaxation time T_1 . **a**, Nuclear spin relaxation time T_1 of ^{115}In as a function of I_{sd} at B_{\perp}

= 3.56 T and $T = 100$ mK. Measurement of T_1 by recording the time revolution of R_{xx} with on-resonance and off-resonance RF irradiation is illustrated in the inset. The solid line is a fit to a single exponential used to determine T_1 . **b**, T_1 of ^{115}In at all spikes around $\nu = 2$ as a function of B_{\perp} .

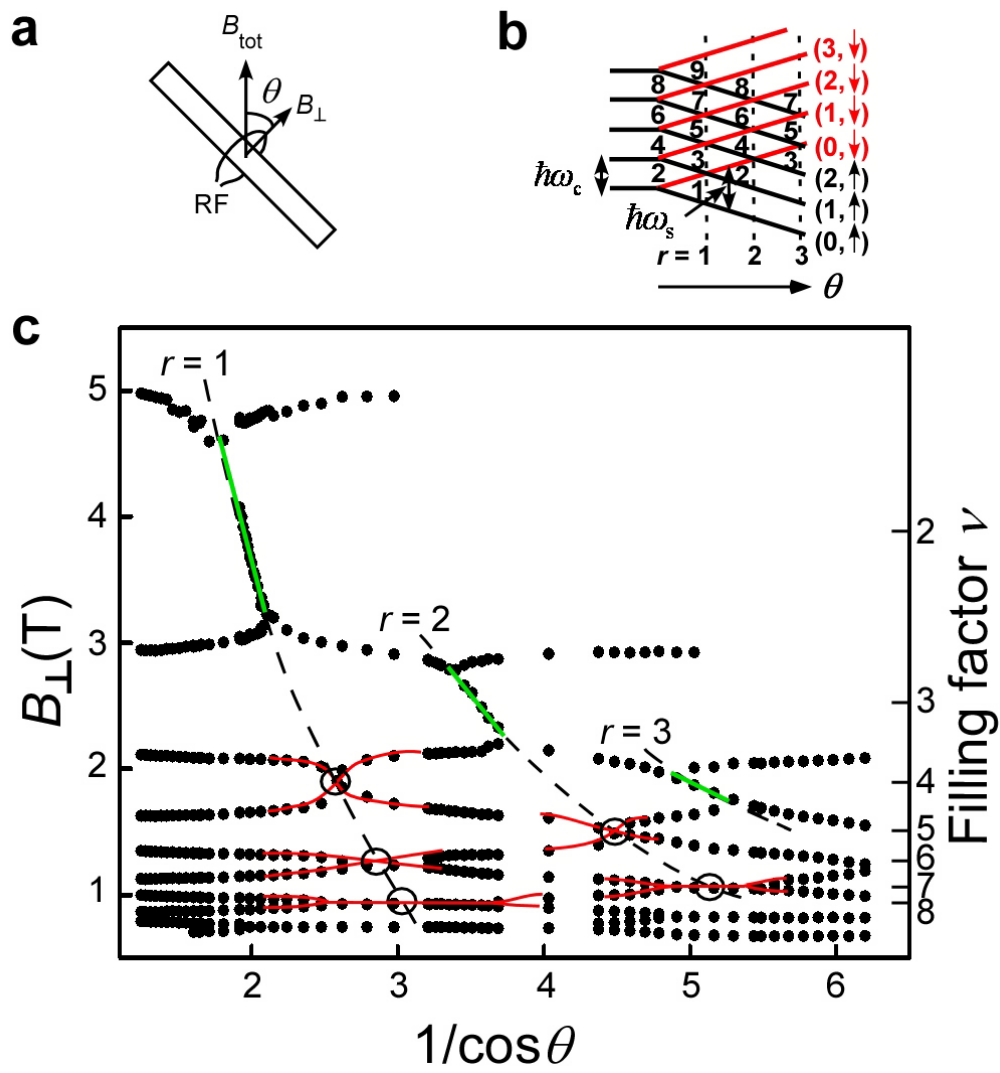


Figure 1

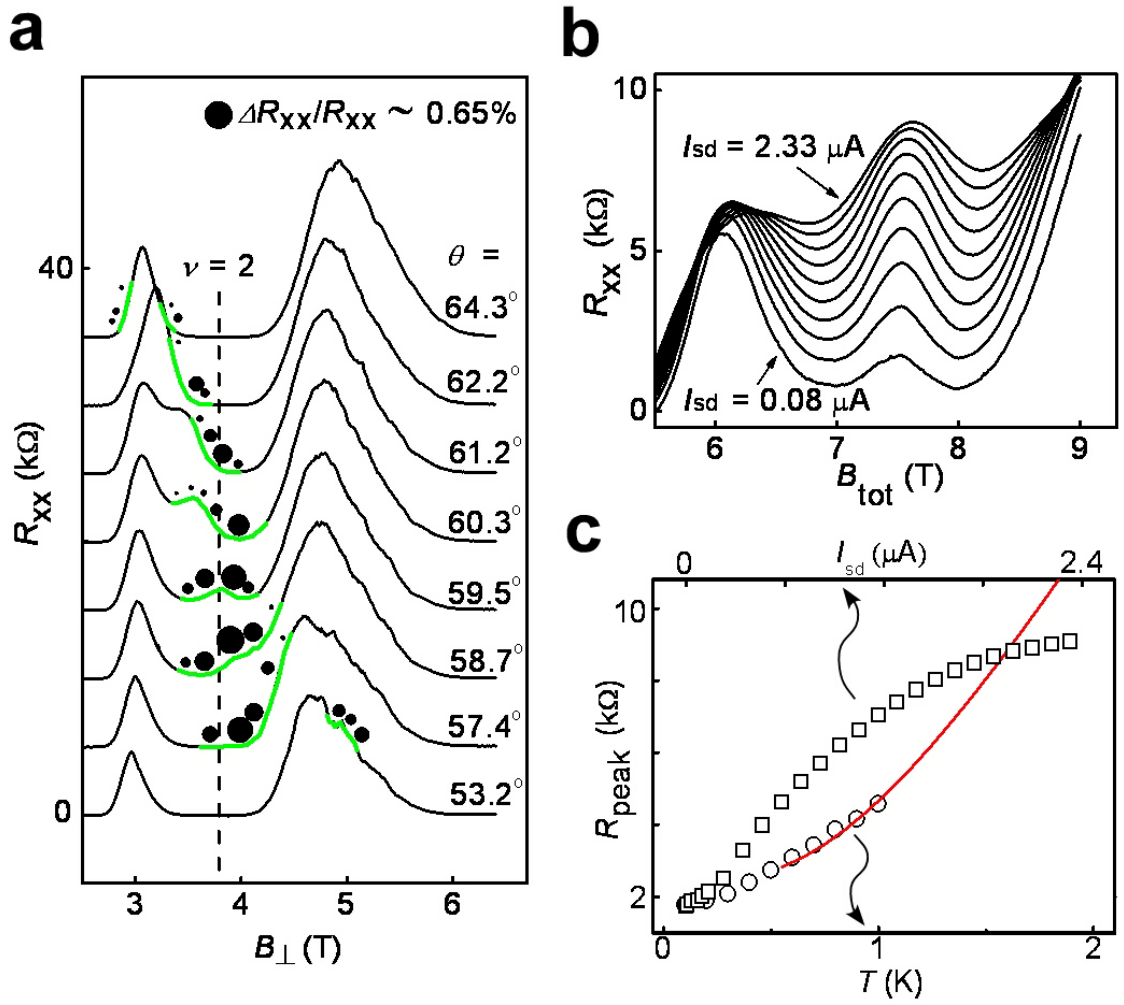


Figure 2

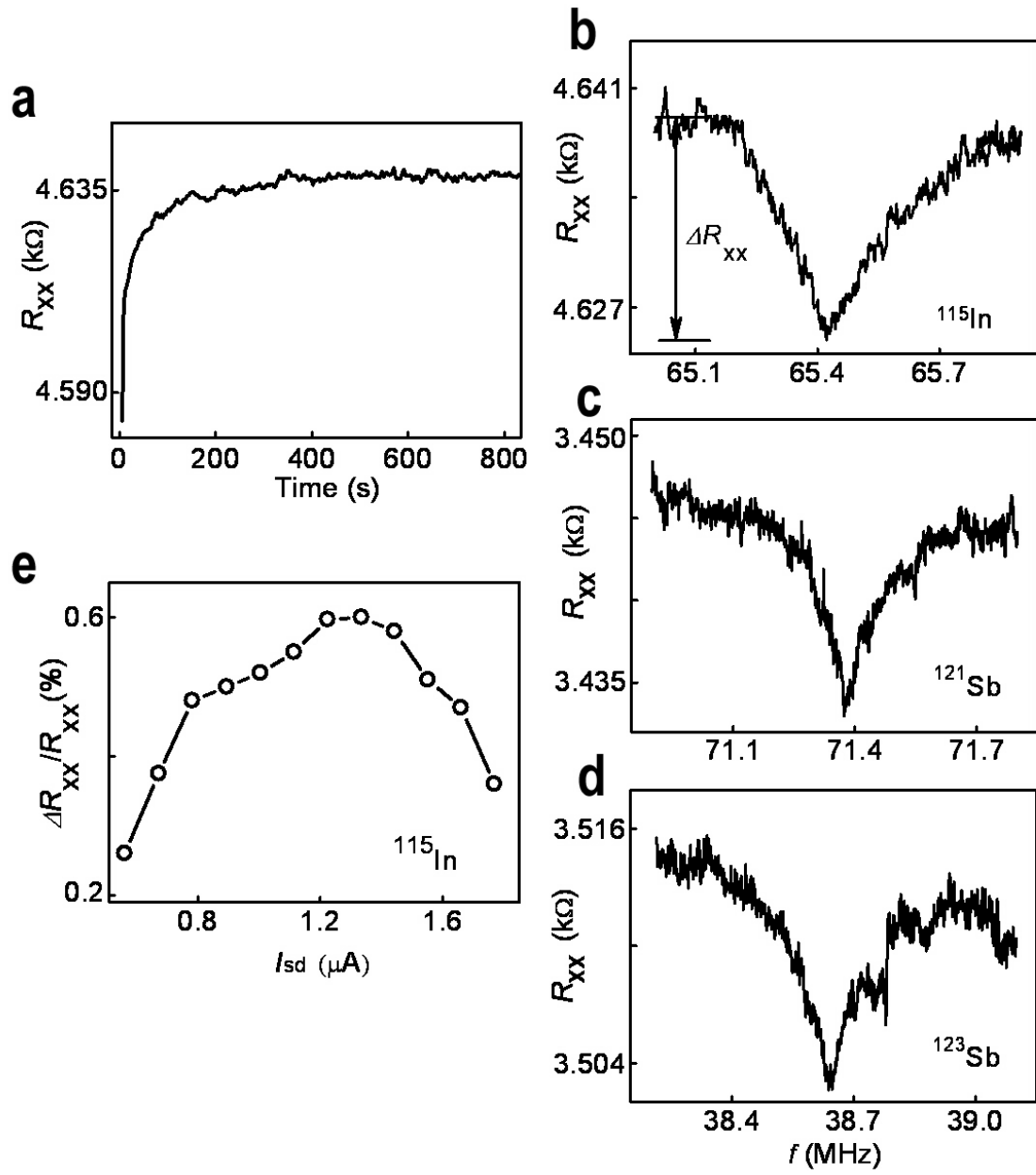


Figure 3

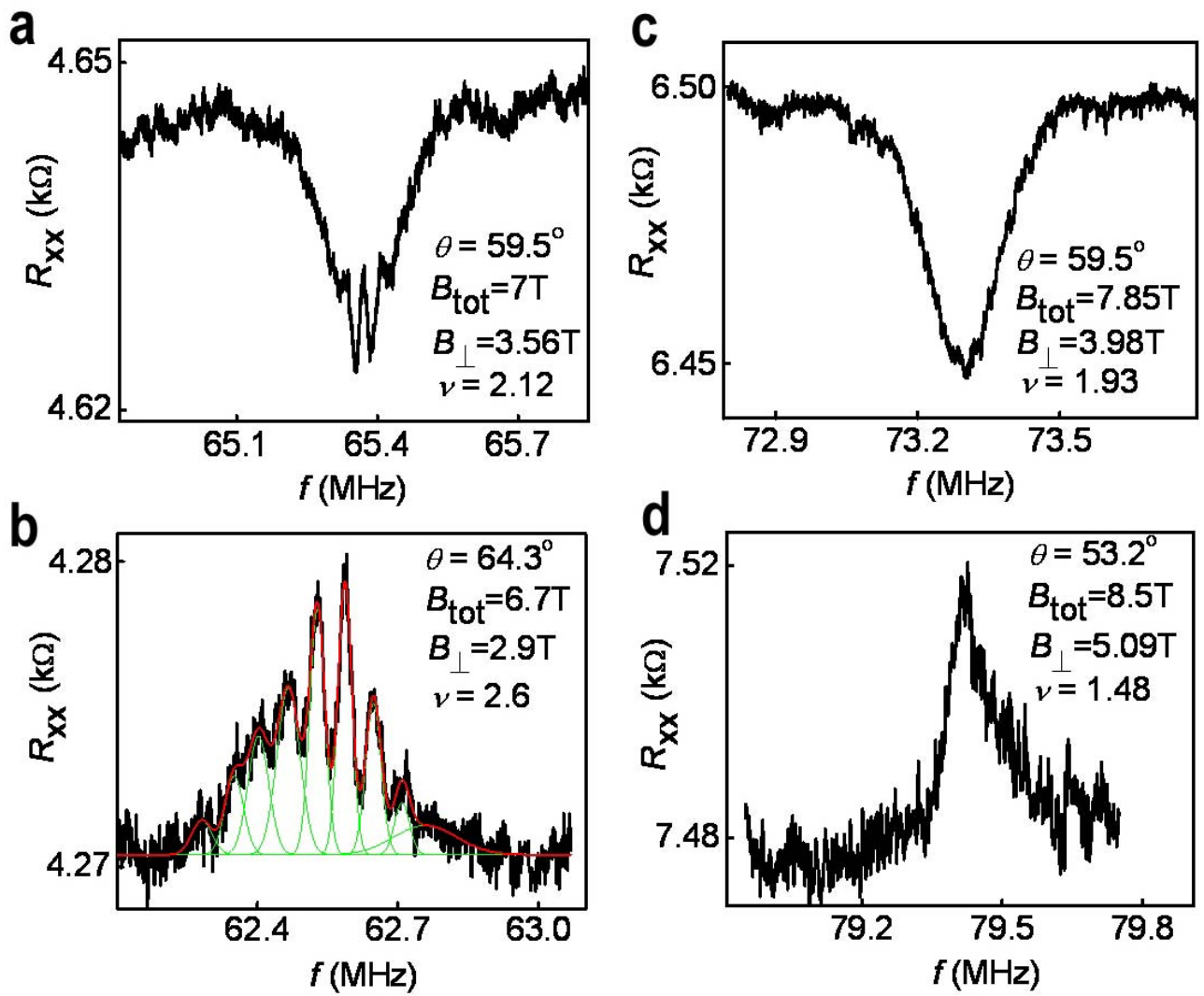


Figure 4

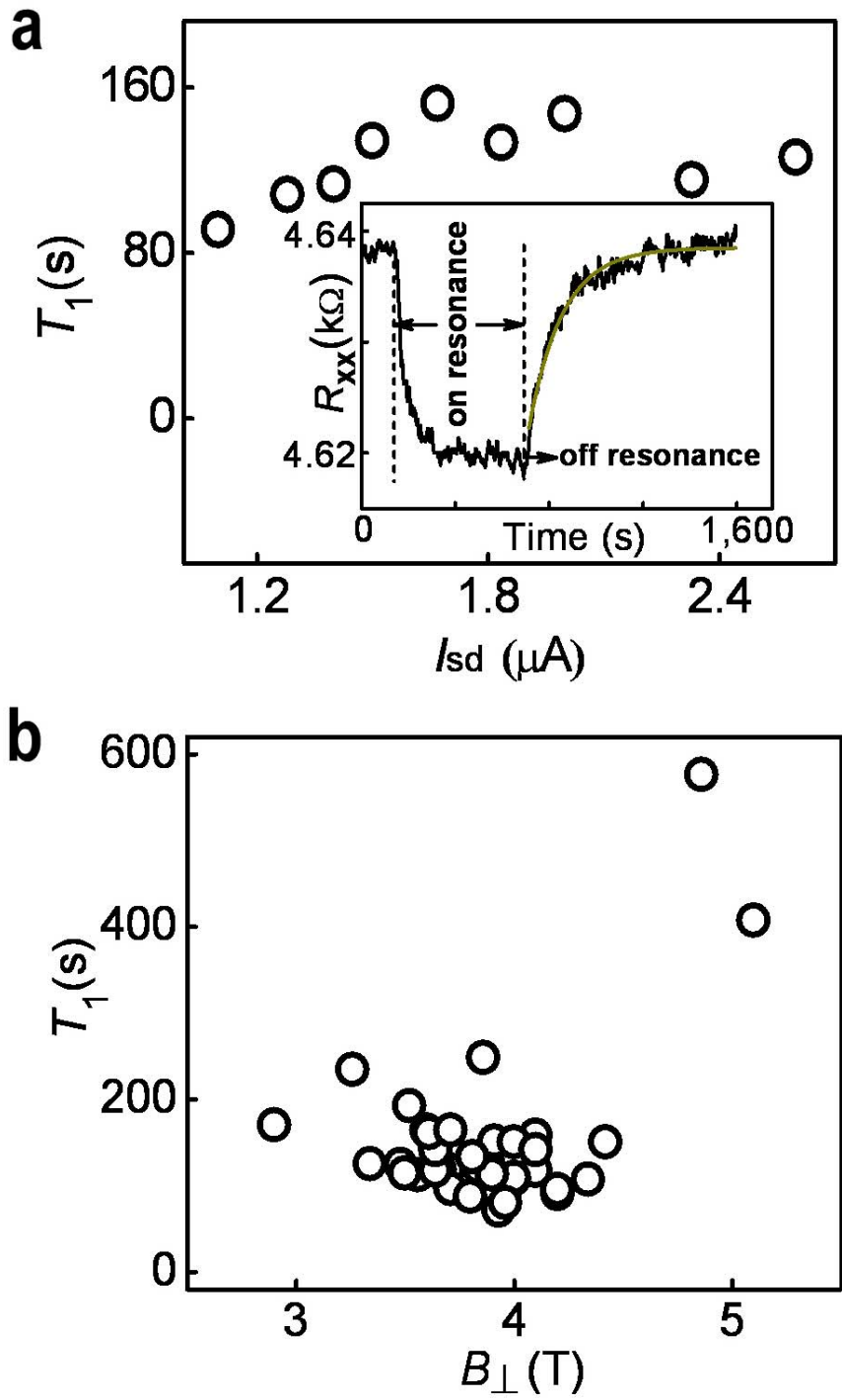


Figure 5